# Gradients of Column $CO_2$ across North America from the NOAA Global Greenhouse Gas Reference Network

Xin Lan[1, 2], Pieter Tans[1], Colm Sweeney[1, 2], Arlyn Andrews[1], Andrew Jacobson[1, 2], Molly Crotwell[1, 2], Edward Dlugokencky[1], Jonathan Kofler[1, 2], Patricia Lang[1], Kirk Thoning[1], Sonja Wolter[1,2]

[1]1National Oceanic and Atmospheric Administration, Earth System Research Laboratory, Boulder, 80303, Colorado, USA

[2] University of Colorado, Cooperative Institute for Research in Environmental Sciences, Boulder, 80309, Colorado, USA

*Correspondence to*: Xin.Lan (xin.lan@noaa.gov)

**Abstract.** This study analyzes seasonal and spatial patterns of column carbon dioxide ($CO_2$) over North America calculated from aircraft and tall tower measurements from the NOAA Global Greenhouse Gas Reference Network from 2004 to 2014. Consistent with expectations, gradients between the eight regions studied are larger below 2 km than above 5 km. The 11-year mean $CO_2$ dry mole fraction ($XCO_2$) in the column below ~330 hPa (~ 8 km above sea level) from NOAA's $CO_2$ data assimilation model, CarbonTracker (CT2015), demonstrates good agreement with those calculated from calibrated measurements on aircraft and towers. Total column $XCO_2$ was attained by combining modeled $CO_2$ above 330 hPa from CT2015 with the measurements. We find large spatial gradients of total column $XCO_2$ during June to August, with north and northeast regions having ~3 ppm stronger summer drawdown (peak to valley amplitude in seasonal cycle) than the south and southwest regions. The long-term averaged spatial gradients of total column $XCO_2$ across North America show a smooth pattern that mainly reflects the large-scale circulation. We have conducted a CarbonTracker experiment to investigate the impact of Eurasian long-range transport. The result suggests that the large summer time Eurasian boreal flux contributes about half of the north-south column $XCO_2$ gradient across North America. Our results confirm that continental-scale total column $XCO_2$ gradients simulated by CarbonTracker are realistic and can be used to evaluate the credibility of some spatial patterns from satellite retrievals, such as the long term average of growing-season spatial patterns from satellite retrievals reported for Europe which show larger spatial difference (~ 6 ppm) and scattered hot spots.

## 1 Introduction

Atmospheric measurements of carbon dioxide ($CO_2$) from ground and airborne platforms have greatly increased our knowledge of the global carbon cycle. Observations of $CO_2$, including the NOAA Global Greenhouse Gas Reference Network (GGGRN), initially emphasized ground-based measurements. These observations, started by C.D. Keeling, have monitored the $CO_2$ trend on both regional and global scales for over 50 years (e.g., Keeling and Rakestraw, 1960; Tans et al., 1989). In addition, the frequency and spatial distribution of airborne measurements have increased rapidly in the last two decades, providing important information about horizontal and vertical variability of atmospheric $CO_2$ (e.g., Gerbig et al., 2003; Choi et al., 2008; Biraud et al., 2013). Routine aircraft

36  measurements from the NOAA/ESRL GGGRN monitor the large-scale distributions of a suite of trace gases,

37  including $CO_2$, under the influence of continental processes (Sweeney et al., 2015). A very successful approach has

38  been to employ commercial aircraft as a platform for $CO_2$ measurements, such as Japan's CONTRAIL

39  (Comprehensive Observation Network for TRace gases by AIrLiner) project, which has provided valuable

40  information for $CO_2$ in the high troposphere and lower stratosphere (Machida et al., 2002; Machida et al., 2008).

41  Vertical profiles of atmospheric $CO_2$ reflect the combined influences of surface fluxes and atmospheric mixing.

42  Vertical profiles are particularly useful for evaluating vertical mixing in atmospheric transport models that are used

43  for inverse modeling (e.g. Stephens et al., 2007) to derive estimates of regional- to continental-scale $CO_2$ sources

44  and sinks (e.g., Tans et al., 1990; Gurney et al., 2002; Gurney et al., 2004; Ciais et al., 2010;).

45  While $CO_2$ sources and sinks are well constrained at the global scale by global mass balance, it remains

46  challenging to accurately resolve $CO_2$ sources and sinks at regional to continental-scale, the apportionment of which

47  depends on relatively minor variations of the observed spatial and temporal patterns of $CO_2$. When averaging over a

48  few months and longer the largest portion of the variations over continents results from hemispheric-scale terrestrial

49  uptake/emissions (photosynthesis)/respiration) and fossil fuel emissions, while regional net fluxes can make a

50  relatively small contribution to the signal. For example, a simple mass balance argument shows that all U.S. $CO_2$

51  emissions from fossil fuel burning (~1.4 Pg yr$^{-1}$) create a total column enhancement of only 0.6 ppm on average in

52  air parcels over the East Coast compared to the West Coast and Gulf Coast if we assume an average of 5 days for the

53  winds to flush the contiguous U.S. (~$8\times10^{12}$ m$^2$).

54  With careful calibration, air handling, and analysis, the uncertainties of in-situ measurements are less than 0.1

55  ppm. However, in-situ observation networks are sparse in global and regional coverage. Remote sensing data

56  radically increase the number of observations and capture under-sampled regions. It could have a valuable impact on

57  our understanding of the carbon cycle. However, both the precision and the potential of even very small systematic

58  biases in remote sensing measurements need to be carefully evaluated, especially those that depend on regional and

59  seasonal conditions. Vertical profiles from in-situ $CO_2$ measurements have been used to evaluate ground-based total

60  column $XCO_2$ (the "X" stands for dry mole fraction) determinations, such as those from the Total Carbon Column

61  Observing Network (TCCON) (Washenfelder et al., 2006; Wunch et al., 2010; Messerschmidt et al., 2011; Tanaka

62  et al., 2012). The uncertainty of TCCON total column $CO_2$ is reported to be 0.4 ppm (1σ) after comparison to

63  aircraft measurements (Wunch et al., 2010). Vertical profiles are also used to evaluate other satellite retrievals of

64  total column $XCO_2$, such as those from the Tropospheric Emission Spectrometer (TES)(Kulawik et al., 2013) and

65  the Greenhouse Gases Observing SATellite (GOSAT) (Inoue et al., 2013, 2016; Saitoh et al., 2016). Satellite

66  retrieval products have known and unknown biases (due to errors in spectroscopy, viewing geometry, spatial

67  differences in clouds and aerosols, surface albedo, etc.) that can result in false horizontal gradients in total column

68  $XCO_2$ for inverse estimates of sources (Miller et al., 2007; Crisp et al., 2012; Feng et al., 2016). After correction for

69  known biases, the mean GOSAT total column $CO_2$ (NIES retrievals) biases range between -2.09 to 3.37 ppm (mean

70  = 0.11 ppm, S.D.= 1.11 ppm; 20 out of 27 stations show biases lower than 1 ppm) across different aircraft sites over

71  land when compared with aircraft-based total column $XCO_2$ (Inoue et al.,2016). The Orbiting Carbon Observatory-

72  2 (OCO-2) retrieval of total column $XCO_2$ was estimated to have a mean difference less than 0.5 ppm from TCCON,

73 with RMS differences typically below 1.5 ppm after bias correction (Wunch et al., 2016). The overall uncertainty of

74 satellite retrievals is relatively large compared with the total column $XCO_2$ calculated from in-situ measurements.

75 Total column $XCO_2$ calculated from vertical profiles from the Japanese CONTRAIL project (Machida et al., 2008)

76 and from the NOAA Carbon Cycle and Greenhouse Gas aircraft program (Sweeney et al., 2015) complemented with

77 simulated profiles from a chemistry–transport model above the maximum altitude of the data have uncertainty less

78 than 1 ppm (Miyamoto et al., 2013). The smaller uncertainty of the in situ-based total column XCO2 suggests that

79 they can be used to evaluate satellite retrievals of column averaged $CO_2$. Since aircraft profiles co-located with

80 satellite retrievals are rare, it is useful to consider the statistics of total column $XCO_2$ fields derived from repeated

81 aircraft profiles over particular locations.

82     The effect of satellite column averaging kernels and a priori profiles when comparing aircraft-based column

83 $XCO_2$ with GOSAT retrievals has been assessed by Inoue et al. (2013). For the case considered, application of the

84 averaging kernel and a priori profile to simulate total column $XCO_2$ was generally within $\pm$ 0.1 ppm of the density

85 weighted total column, suggesting that the averaging kernels can only account for small part of the overall

86 uncertainty of the GOSAT total column $XCO_2$ (Inoue et al., 2013).

87     Transparent and objective estimates of $CO_2$ sources and sinks derived from atmospheric measurements are

88 essential for validating emissions reduction efforts and other mitigation policies, and for lowering the uncertainties

89 of carbon cycle-climate feedbacks. The latter are major ambiguities in predicting future climate, such as potential

90 uncontrolled $CH_4$ and $CO_2$ emissions from warming permafrost in Arctic regions. Satellite retrievals of total column

91 $XCO_2$ can significantly improve estimates of sources and sinks only if they are sufficiently precise and accurate (

92 Houweling et al., 2004; Chevallier et al., 2014), meaning that even very small systematic errors (biases) must be

93 eliminated. Here, we analyze the spatial and temporal variability of column $CO_2$ over North America using well-

94 calibrated $CO_2$ measurements from aircraft and tall tower, and we use model results from NOAA's CarbonTracker,

95 version CT2015 (Peters et al. 2007, with updates documented at http://carbontracker.noaa.gov) to investigate the

96 primary drivers of variability in total column $XCO_2$. The aircraft data enable direct analysis of column $CO_2$

97 characteristics, which is the fundamental step for accurate apportionment of sources and sinks. This study focuses on

98 long-term averaged column $CO_2$ gradients and the contributions of different vertical layers to the total column

99 variability. It can serve as a reference for evaluating regional and seasonal biases of current and future column $CO_2$

100 retrievals from both ground and satellite platforms.

101 **2 Methods**

102 **2.1 Aircraft and tall tower sampling**

103 Aircraft sampling in the NOAA GGGRN intends to provide vertical profiles of long-lived trace gases to capture

104 their seasonal and interannual variability. The aircraft sampling system consists of 12 borosilicate glass flasks in

105 each programmable flask package (PFP), a stainless-steel gas manifold system, and a data logging and control.

106 These flasks (0.7 L each) are pressurized to obtain 2.2 L of sample air from each target altitude. Air samples are then

107 shipped back to NOAA/ESRL for carefully calibrated and quality-controlled measurements. Carbon dioxide is

108  measured using a nondispersive infrared analyzer. Long-term measurements at ~15 sites are carried out using light

109  aircraft that can reach 8.5 km. Air samples are collected mostly during late morning to early afternoon, when the air

110  mass within the planetary boundary layer (PBL) is generally well mixed, and $CO_2$ enhancement near the ground

111  from plant respiration during the night has been mixed throughout the boundary layer. Normally, the aircraft follows

112  a pre-decided route such that most samples are collected within 0.1° of the site location. The sampling frequency

113  varies from site to site, currently from twice a month to once every 1.5 months. For more sampling details, quality

114  control discussions, and an evaluation of the sampling frequency, please refer to Sweeney et al. (2015). More

115  information on the aircraft sites can be found at http://www.esrl.noaa.gov/gmd/ccgg/aircraft/. We estimate the

116  uncertainty of individual measurements of $CO_2$ in flask air (68% confidence level) at 0.08 ppm. However, we have

117  seen evidence of positive biases for samples collected using older flasks that may contain contaminants. Andrews

118  et al. (2014) reported biases that increased from <0.1 ppm in 2008 to an average offset in 2013 of 0.36 ppm. The

119  aircraft sampling protocol was modified starting in August 2014 to mitigate this bias. For samples collected prior the

120  protocol change, laboratory tests showed that new/clean flasks have zero bias, but some older/dirty flasks could have

121  biases of > 1 ppm. This bias is not consistent among individual flasks and increasing over time (Andrews et al.,

122  2014), the potential bias is hard to quantify for measurements before August 2014. Thus, the high bias is not

123  corrected in our study. More recently, low bias has been found in PFP measurements when the ambient humidity is

124  high, based on comparisons of PFP measurements with data from in-situ analyzers at tall towers. We are working to

125  understand and quantify this bias, and for this study we have derived a preliminary correction factor, which shows a

126  linear trend with −1.4 ppm $CO_2$ offset per 1% above 1.7% of ambient water (mole fraction relative to whole air)

127  content. Only ~ 4% of total aircraft measurements or ~ 12% of those below 2 km are impacted by humidity higher

128  than 1.7%, for which we have applied corrections before data analysis. The mean correction applied is 0.53 ± 0.4 (1

129  σ) ppm for the impacted data.

130  The NOAA tall tower network measures $CO_2$ and other trace gases within the continental boundary layer.

131  Continuous in-situ measurements are conducted using nondispersive infrared (NDIR) absorption sensors and cavity

132  ring-down analyzers. The long-term stability of these systems is typically better than 0.1 ppm for $CO_2$ (Andrews et

133  al., 2014). Most tall tower sites have more than one air intake height. In this study, continuous in-situ measurements

134  from the highest intake are used to minimize potential influences from local sources. More information concerning

135  the tower sites can be found at http://www.esrl.noaa.gov/gmd/ccgg/insitu/. For the column $XCO_2$ calculation, tower

136  data only from 10:00-17:00 local standard time (LST) on flight days are averaged to one data point per day, as a

137  complement to vertical profiles within the PBL.

138  **2.2 Site description**

139  We analyze data from 19 aircraft sites and 6 tall tower sites during 2004 to 2014 (see Table S1 for a summary of site

140  conditions). After considering the geographic distribution of these sites in North America, we group them into eight

141  regions for spatial comparisons (Fig. 1). The northern west (NW) and southern west (SW) regions represent the

142  inflow area in the west coast of US, directly downwind of the Pacific Ocean at both higher elevations. The northern

143  mid-continent (NM) region represents the boreal forest and agriculture region in north-central North America. The

144    mid-continent (MC) region represents a dry landscape due to its high elevation (above 1.5 km on average) and semi-

145    arid climate. The mid-west (MW) region is strongly influenced by agriculture and temperate forest.  The southern

146    mid-continent (SM) represents the south-central humid temperate region, with inflow from the Gulf of Mexico

147    during summer.  The northeast (NE) region represents the temperate forest in north-east coast of U.S., which is

148    mostly downwind of regions to the west above the PBL, and downwind of its south-west regions within the PBL.

149    The southeast (SE) region represents the warm temperate region in the south-east coast of U.S.

150

151
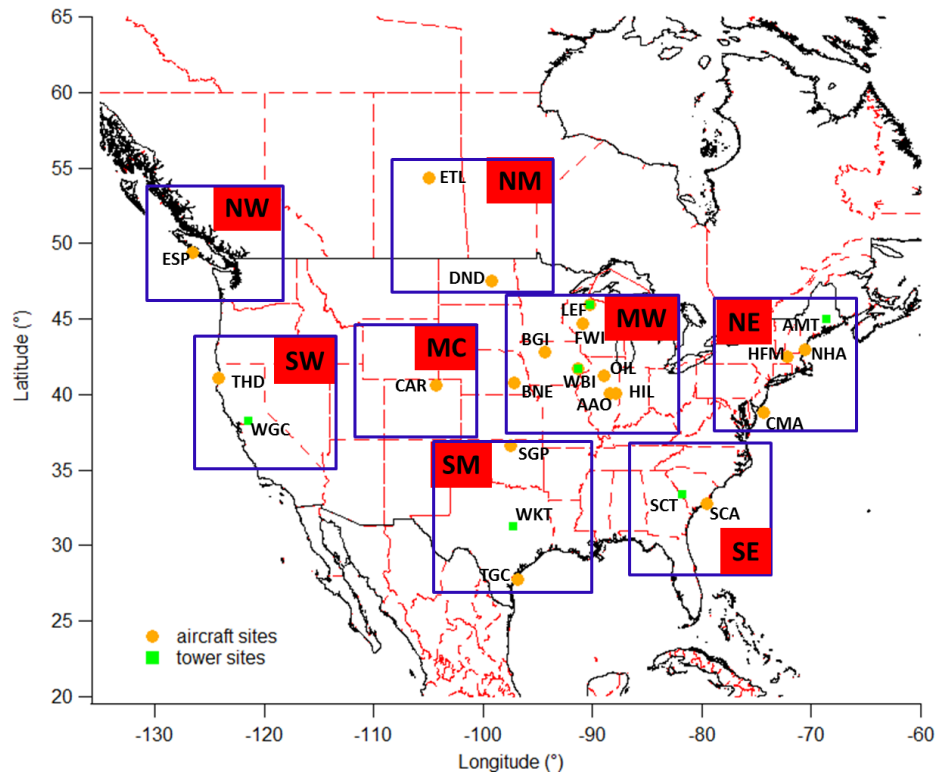
152    **Fig. 1.** Aircraft, tall tower, and high elevation/tower sites in the NOAA GGGRN. The eight boxes define regions

153    that are further discussed for spatial pattern comparison.

154    **2.3 Smoothing of the reference data and column XCO$_2$ calculation**

155    We use Mauna Loa Observatory (MLO) as a reference site. MLO is located at 19.536°N, 155.576°W, and 3397 m

156    above sea level. Carbon dioxide measurements from this site are widely used to represent background CO$_2$ in the

157    Northern Hemisphere. For our study, a function consisting of a quadratic polynomial and four harmonics is fitted to

158    the MLO data, adopted from the method described by Thoning et al. (1989). Residuals of the data from this function

159    are smoothed by a low-pass filter with full-width at half-maximum in the time domain of 1.1 years. The smoothed

160    residuals are then added back to the polynomial part of the function to produce the long-term deseasonalized trend.

161    This trend (see Fig. 3) is subtracted from all aircraft and tall tower measurements. Also, the CarbonTracker results

162    presented in this study are the differences relative to observed MLO deseasonalized trend. We use '∆' to represent

163    detrended data in the following text and figures.  The choice of reference site is not important for this study, since

we focus on examining the relative seasonal patterns of the detrended spatial and vertical distributions of $CO_2$ instead of the total changes in $CO_2$ abundance attributed to global surface fluxes.
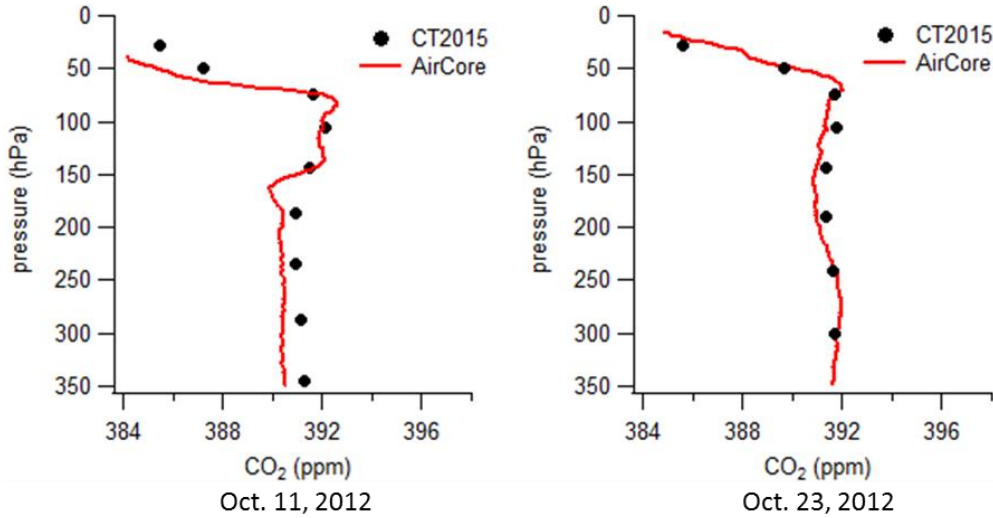
**Fig. 2**. Carbon Tracker (CT2015) simulations compared with AirCore in-situ measurements in upper atmosphere. AirCore profiles in the left and right panels are sampled near CAR and SGP, respectively.

We calculate partial column average $CO_2$ dry mole fraction using tall tower and aircraft data, and the total column by adding simulations of high altitude $CO_2$ (above 330 hPa, ~ 8 km above sea level) from CarbonTracker. Since geometric height from the onboard Global Positioning System (GPS) (after 2006) or inferred from the aircraft altimeter or pressure altitude is archived with each aircraft measurement, we first convert geometric height (in meter) to pressure (in hPa) for the pressure-weighted column $XCO_2$ calculation. This conversion uses geopotential data from NOAA/NCEP North American Regional Reanalysis (NARR) (Mesinger et. al, 2004), available at https://www.esrl.noaa.gov/psd/data/gridded/data.narr.html, in which the geopotential is a function of latitude, longitude, pressure altitude and time. We interpolate the geopotential field vertically to retrieve pressure, and then calculate dry pressure by incorporating specific humidity data from NARR. Eventually we use a trapezoidal method to integrate over detrended vertical profiles for dry-pressure-weighted column averages. For the long-term averaged column $\Delta XCO_2$ calculation, a long-term mean vertical profile is first constructed for each month by combining 11-year detrended data together and then average data in each 40 hPa vertical bin. To look at the long-term averaged total column $\Delta XCO_2$ from individual aircraft sites, we combine aircraft data with upper-layer CT2015 simulations.

The NOAA CarbonTracker model assimilates $CO_2$ measurements from surface sampling networks and tall towers to generate global 3D fields of atmospheric $CO_2$ mole fraction. The Carbon Tracker model has evolved significantly since Peters et al. (2007). A detailed description of this model is provided in documents available at http://carbontracker.noaa.gov. Our study utilizes CarbonTracker results from the 2015 release (CT2015), publicly accessible at ftp://aftp.cmdl.noaa.gov/products/carbontracker/co2/CT2015/molefractions/. This version provides $CO_2$ mole fraction over North America with $1° \times 1°$ spatial and 3 hour temporal resolutions, which are analyzed in

190   Sect. 3.2 and 3.3. Total column $CO_2$ calculated from CT2015 global data with $3° \times 2°$ spatial resolution is also

191   presented in the supporting information (SI). We have evaluated the performance of CarbonTracker in upper

192   atmosphere (330 to 0 hPa) by comparing its simulations with in-situ measurements from 9 AirCore profiles (Karion

193   et al., 2010) sampled in 2012-2014. AirCore is a ~150 m stainless steel tube that utilizes changes in ambient

194   pressure for passive sampling of the vertical profile. The tube is carried to high altitude by  balloon and it collects a

195   continuous sample as it descends. It is then measured by an analyzer after it is recovered. More information about

196   AirCore system can also be found at https://www.esrl.noaa.gov/gmd/ccgg/aircore/. All 9 AirCore profiles are taken

197   near SGP and CAR sites. Figure 2 shows examples of AirCore profiles compared with CT2015 in the upper

198   atmosphere, which demonstrates good agreement. We also compare partial column (330 to 0 hPa) averages from the

199   9 AirCore profiles and CT2015. Results from CT2015 agree generally well with AirCore, with difference ranging

200   from 0.03 to 1.22 ppm (mean value equals 0.66 ppm), which suggests that CT2015 may have a high bias that could

201   contribute to $0.66\times1/3=0.22$ ppm overestimate on average to the total column average.  However, AirCore is in the

202   process of rigorous evaluation, the differences between AirCore and CT2015 are not well characterized yet since we

203   only have a limited amount of AirCore data. It is unclear whether the potential bias of CT2015 in this partial column

204   is dependent on time or sampling location. Adding a constant bias correction to all regions will not change the

205   spatial gradients that we focus on in this study. Thus no correction is applied when using CT2015 simulations to

206   represent the upper 1/3 of the total column. For uncertainty estimates, we use a ''bootstrap'

207   method that uses random resampling of individual vertical profiles with restitution (low bias, high humidity was

208   corrected), with 100 Monte Carlo runs for each column average calculation. Uncertainty is then defined as one

209   standard deviation of the 100 Monte Carlo results.

210   **3 Results and Discussions**

211   **3.1 Seasonal patterns and spatial gradients**

212   Typically one aircraft profile contains measurements at 12 different altitudes. Column $\Delta XCO_2$ can be computed for

213   each profile using the method described in Sect. 2.3 (Fig. S1). Our aircraft and CT2015 based column $CO_2$ at SGP

214   and LEF sites shows reasonable agreements with TCCON data retrieved at Lamont and Park Falls site

215   (Washenfelder et al., 2006; Wunch et al, 2009, 2011), respectively (Fig. S2). Figure 3 shows aircraft (at all altitudes)

216   and tower data (daily averages for 10:00-17:00 LST data) from all sites used in this study. Aircraft data above 2 km

217   exhibit much smaller seasonal variations than the full dataset, because the variations are mainly driven by $CO_2$

218   sources and sinks near Earth's surface.  $CO_2$ mole fraction is enhanced in the shallow wintertime PBL primarily due

219   to reduced plant photosynthesis and ecosystem respiration combined with slightly increased fossil fuel emissions.

220   During summer the PBL is deeper, and depletions within the PBL are due to strong terrestrial uptake that dominates

221   over emissions especially during June through August. During summer of 2010 to 2012, $CO_2$ from aircraft

222   measurements appears higher than other years in Fig.3; however, similar characteristics are not present in tower

223   data. This apparent difference is due to a decrease in sampling frequency at several aircraft sites that resulted in an

224  aliased picture of the full summer signals. Since we focus on climatological mean of 11 years of data in our study,

225  this influence is eliminated by combining 11 years of data together into one "average year".

226
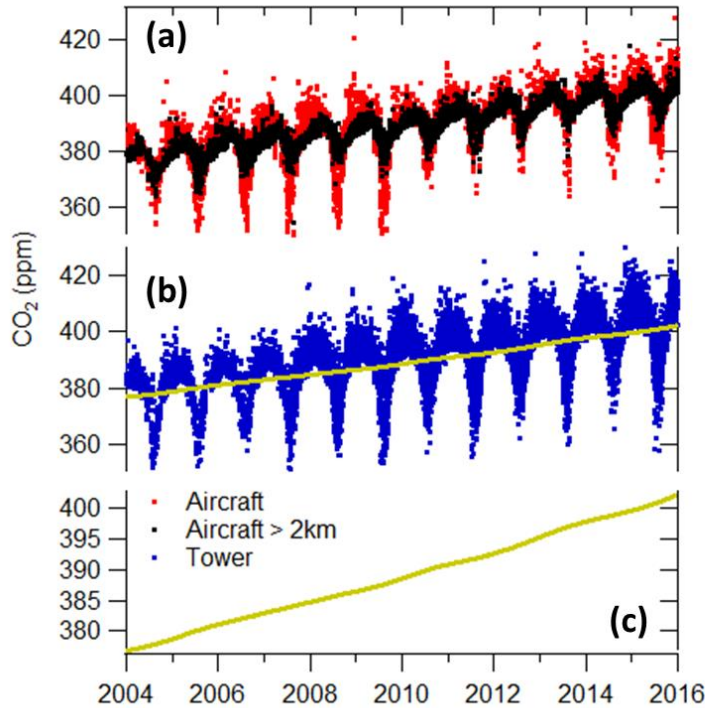
227  **Fig. 3.** $CO_2$ observations from aircraft (a) and towers (b). The yellow line in (b) illustrates the deseasonalized trend

228  at Mauna Loa (MLO), same as in (c), in which y-axis is expanded.

229

230      To investigate the contributions of different altitudes to spatial gradients between regions, we divided all

231  measurement data into three layers according to their sampling altitudes: below 2 km, 2 - 5km, and 5 - 8.5 km masl

232  (Fig. 4). Smooth seasonal curves are attained from fitting data with four harmonics using the method described by

233  Thoning et al. (1989). The peak-to-valley amplitudes of the seasonal cycles below 2 km are the largest among the

234  three layers for most regions, with a minimum of 10.3 ppm in SM and a maximum of 25.0 ppm in MW. The

235  seasonal variation amplitudes decrease to 7.7-11.5 ppm in the 2 - 5 km layer, and further decrease to 7.2-10.0 ppm in

236  the 5 - 8.5 km layer. We also observe that the seasonal cycle drawdown occurs later in the layers above 2 km (see

237  Fig. S3, which provides similar information as Fig. 4, but seasonal curves from different vertical layers are grouped

238  by regions to facilitate comparisons of the phases of seasonal cycles). The seasonal $CO_2$ drawdown below 2 km is

239  mainly influenced by terrestrial photosynthesis and gradients are due to local to regional fluxes, with an earlier onset

240  of drawdown in southern regions than in northern regions. The seasonal cycle aloft is damped and lagged compared

241  to the PBL, with influences from throughout the Northern Hemisphere and with spatial gradients likely driven by

242  large-scale transport. The NW, SW, SM, and SE inflow regions have significant delays of more than one month in

243  the 2 - 5 km layer compared with the surface layer, which is likely due to the delayed phase of the seasonal cycle in

244    well-mixed air coming from the oceans. Vertical homogeneity of air over ocean was observed during the HIAPER
245    Pole-to-Pole Observations (HIPPO) aircraft campaign (Wofsy et al., 2011; Frankenberg et al., 2016). As air masses
246    are transported further inland, we observe reduced discrepancies of the timing of $CO_2$ drawdown between surface
247    and upper layer air (2-5 km), which may be associated with the increased influence of the land surface in the mid-
248    troposphere due to strong convection over land. $CO_2$ drawdown in the 5 - 8.5 km layers also occurs later than in the
249    2 - 5 km layers in most regions; however, differences between these two layers are small. The declining amplitude
250    and delayed phase of the seasonal cycle with altitude have been noted often (e.g., Tanaka et al., 1983; Ramonet et
251    al., 2002; Gerbig et al., 2003, Sweeney et al. 2015). It demonstrates that there is lot of important information in the
252    vertical profile that is diminished in observations of the total column.

253    We find that the largest horizontal spatial gradients between regions occur below 2 km during summer time
254    (Fig. 4), with a maximum difference of ~15.5 ppm between MW and SM. SM and SW exhibit less pronounced
255    seasonal cycles, which is likely associated with air masses from the Gulf of Mexico and the Pacific Ocean,
256    respectively, whereas MW exhibits a deep summer drawdown (amplitude in seasonal cycles) partially as a result of
257    strong regional forest and crop uptake. Crevoisier et al. (2010) estimated the surface flux over North America using
258    vertical $CO_2$ measurements and average wind vectors,  and reported that annually averaged land carbon fluxes in the
259    western (including SW region) and southern regions (including SM region) were neutral. The SE region also
260    demonstrates a less pronounced seasonal cycle with higher summertime levels compared with other northern
261    regions, which may be due to the sea-breeze influence in summer within PBL. In wintertime, $CO_2$ levels in NE and
262    MW are higher than in other regions, which result from regional fossil fuel and terrestrial biogenic emissions
263    combined with transport from the west and south.

264    Higher altitude data (above 2 km) exhibit only small spatial gradients. In the 2 - 5 km layer, the largest gradient
265    is 4 ppm in summer (Fig. 4b). It further decreases to less than 3 ppm in the 5 - 8.5 km layer (Fig. 4c).  Figure 4d
266    shows modeled $CO_2$ mole fractions from CT2015 for the upper troposphere and above (330 hPa to 0 hPa), which are
267    used to fill in above the aircraft profiles for calculation of total column $\Delta XCO_2$. Spatial gradients in this layer are
268    less than 0.5 ppm, suggesting that the top third of the total column has little contribution to the spatial gradients of
269    the total column.
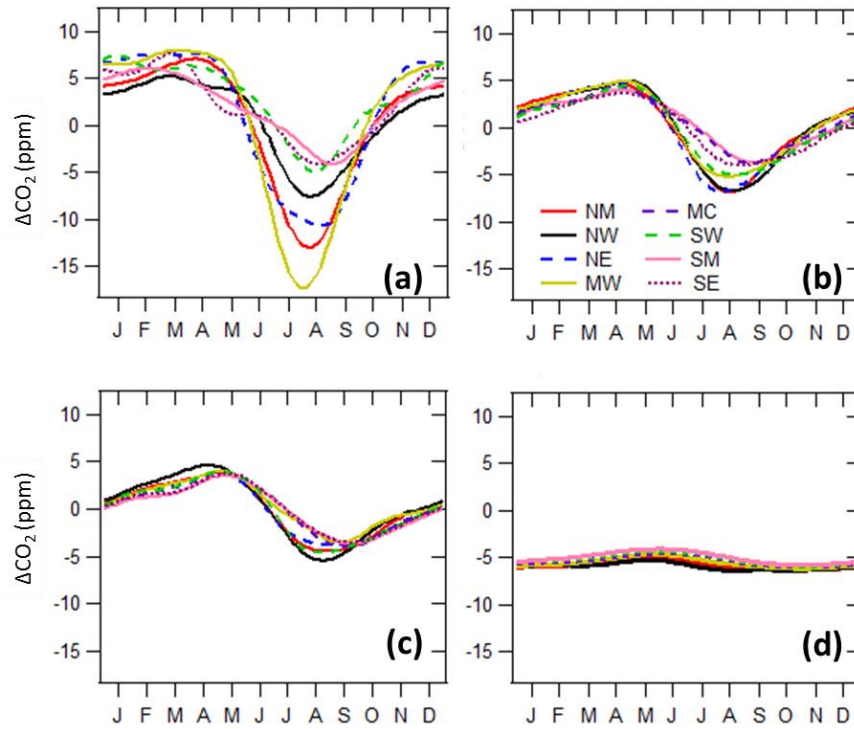
**Fig. 4.** Multi-year (2004-2014) average smooth seasonal curves of $CO_2$ relative to the long-term de-seasonalized trend at Mauna Loa for different vertical layers: (a). Aircraft and tower data under 2 km, MC is not presented because only limited data were available due to high surface elevations (>1.5 km on average) in this region; (b). Aircraft data from 2 - 5 km; (c). Aircraft data from 5 - 8.5 km; (d). CT2015 model results for layers above 330 hPa (~8.5 km) to 0 hPa (~80 km).

**3.2 Long-term mean vertical profiles**

To investigate the mean spatial gradients, we first calculate the long-term mean monthly vertical profiles as described in Sect. 2.3. In addition, each tower serves as one additional layer in the mean profile. The long-term mean tower data generally fit well in the vertical profiles from measurements of aircraft samples (Fig. 5 and Fig. 6), suggesting that the biases described in Sect. 2.1 above do not significantly affect the long-term mean. To attain profiles of the entire atmospheric column, upper layers (330 to 0 hPa) are filled in by CT2015, and the lowest data point of the measured profile is extended to ground level, defined by the mean surface elevation in that region.

Figure 5 presents two examples of long term mean profiles with data variability, which is the one standard deviation for each 40 hPa bin of aircraft data or for all flight-day tower data. Variability as large as 20 ppm is seen within the PBL in the MW region in summer, which is due to strong and heterogeneous surface vegetation uptake and ecosystem respiration combined with day-to-day changes in wind direction. All long-term mean monthly vertical profiles are presented in Fig. 6, which shows the mean temporal and vertical variability of $CO_2$ in each season, and further demonstrates the vertical propagation of seasonal $CO_2$ due to changes of surface flux. In

289    wintertime, monotonic decrease of $CO_2$ with altitude can be observed from all regions, in which high PBL $CO_2$ is

290    mainly driven by surface emissions and reduced vertical mixing (Denning et al., 1998; Stephens et al., 2007).

291    Surface $CO_2$ decreases dramatically in the growing season in those regions influenced by high plant activity, such as

292    NM and MW regions. For the summer vertical profiles in NE and SE region (east coast of the U.S.), the $CO_2$ mixing

293    ratio is elevated in the layer under 900 hPa followed by significant decreases in upper layers until 750 hPa, and then

294    increases with altitude until tropopause (Fig. 6). This is likely a result of sea breeze influence. Lower-troposphere air

295    from the sea, lacking terrestrial uptake of $CO_2$, typically has higher $CO_2$ in summer compared with inland air.

296    Polluted air previously advected offshore can be brought back along with sea breeze. Without significant vertical

297    mixing over the marine surface, high levels of pollutants remain in those air masses. The convergence of sea breeze

298    with prevailing wind moving offshore may create a period with a stalled frontal structure that can aggregate air

299    pollutants (Banta et al., 2005). The convective internal boundary layer structure of the sea breeze system can

300    significantly reduce mixing height (Miller et al., 2003), and also induces higher $CO_2$ levels.  When the sea breeze is

301    not dominant, air advected from southwest and west (the land) can also bring in polluted air with high $CO_2$ since this

302    region is downwind of continental U.S. emissions (Miller et al., 2012).

303
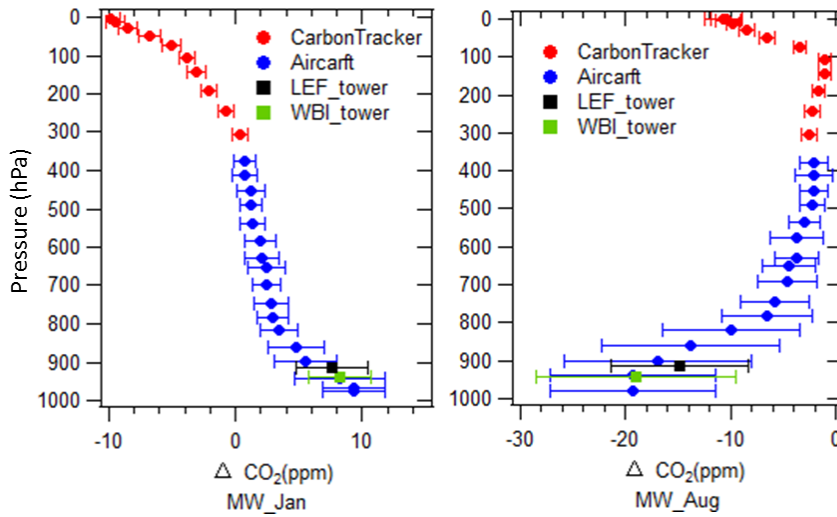
304    **Fig. 5**. Long-term mean (2004-2014) average vertical profiles in January (left panel) and August (right panel) in

305    region MW. Error bar shows one standard deviation.
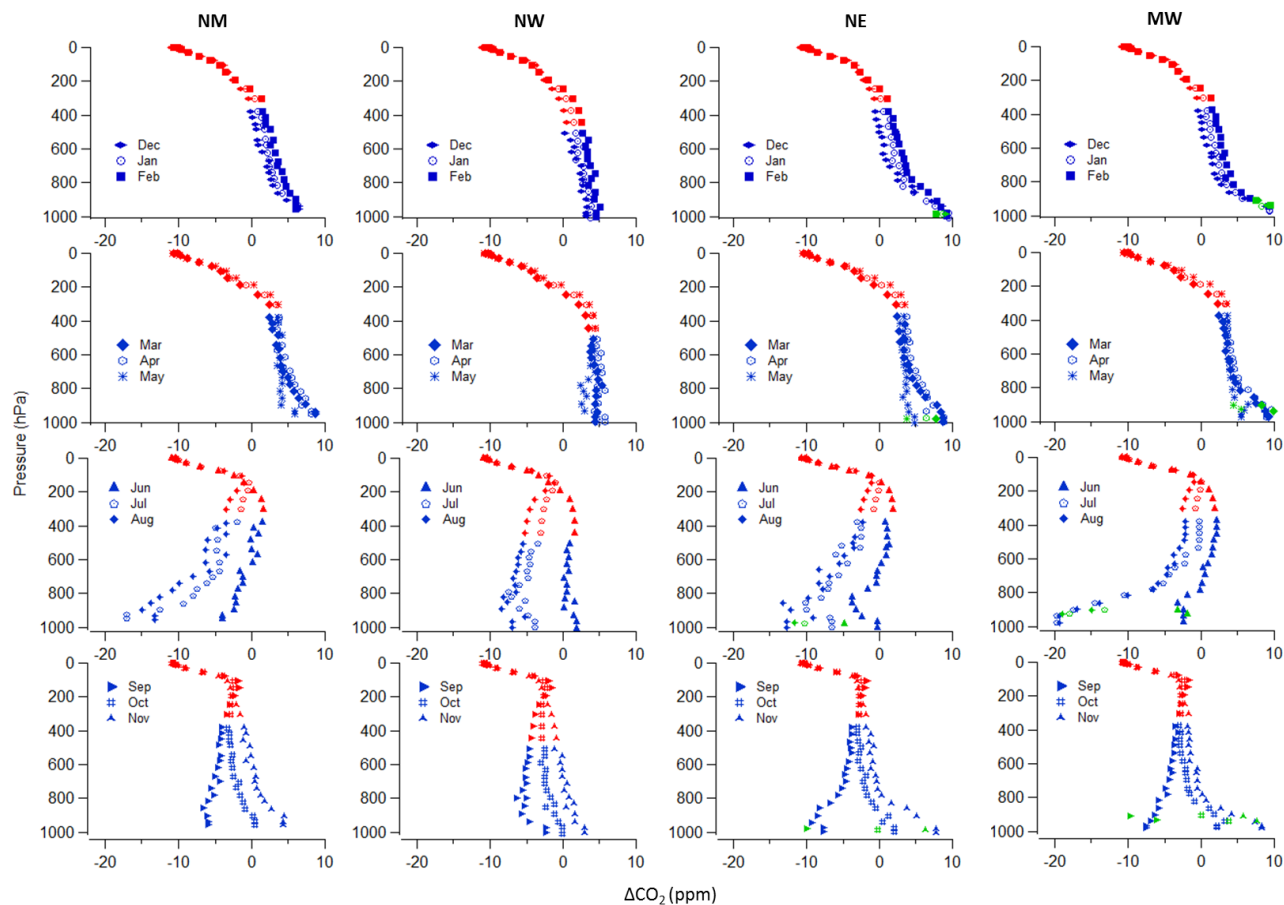
306

307 **Fig. 6a**. Long-term mean (2004-2014) monthly vertical profiles in NM, NW, NE, MW (by column, from left to

308 right). Blue points were calculated from observations, red points were calculated from CT2015, and green points

309 were calculated from tower data.

310
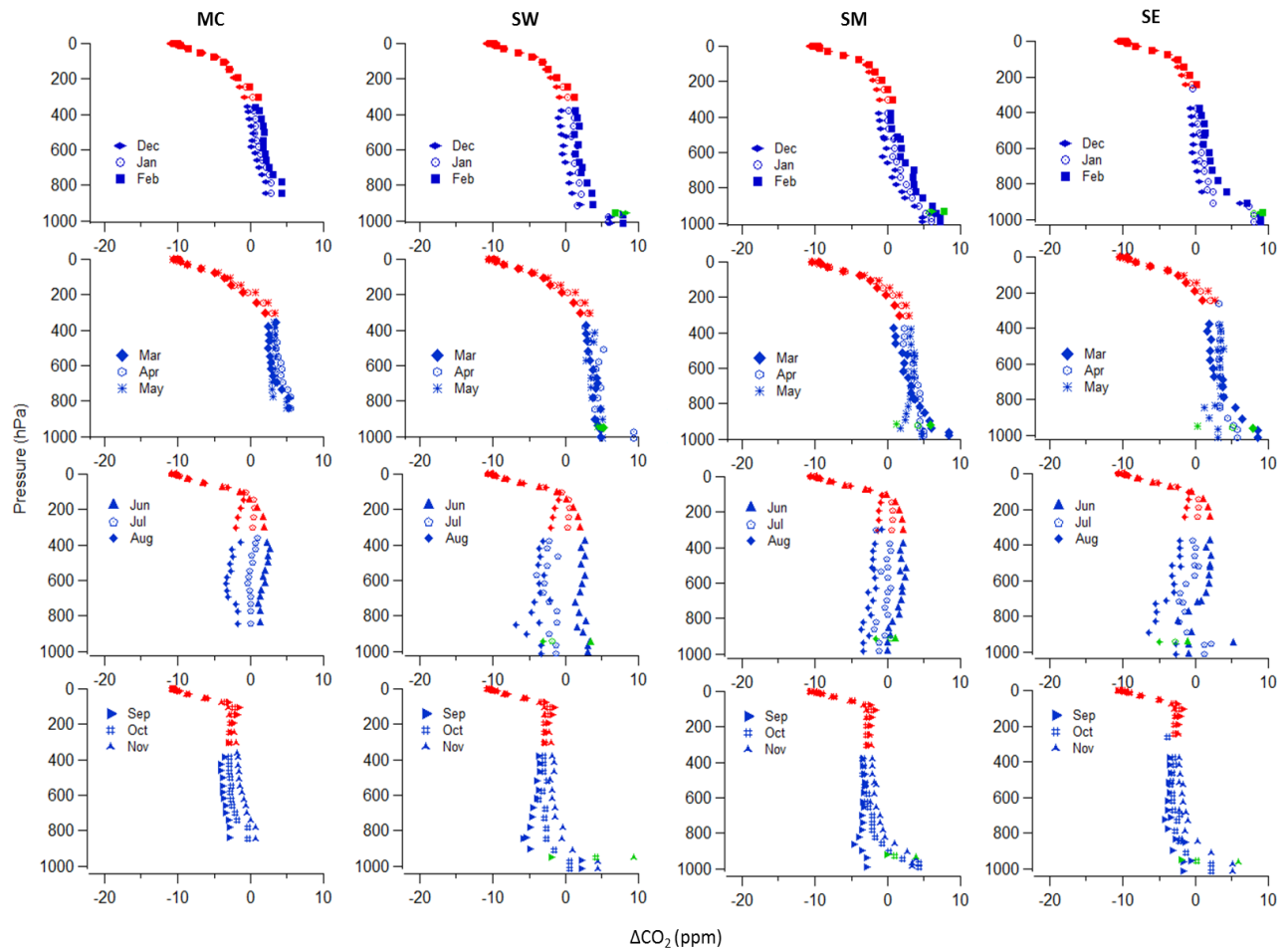
**Fig. 6b**. Long-term mean (2004-2014) monthly vertical profiles in MC, SW, SM, SE (by column, from left to right). Blue points were calculated from observations, red points were calculated from CT2015, and green points were calculated from tower data.

314

## 3.3 Partial column $\Delta XCO_2$ and total column $\Delta XCO_2$

Seasonal variations of monthly averaged partial column $\Delta XCO_2$ (below 330 hPa) demonstrate maximum values in April and minimum values in August or September (Fig. 7a). The largest amplitude appears in NM, with peak-to-valley difference up to 13.5 ppm. SW, SM, SE, and MC have similar amplitudes of 7-8 ppm, smaller than the other three regions. To evaluate the performance of CT2015 on column $\Delta XCO_2$, CT2015 results are sampled to match the latitude, longitude, altitude and time of actual measurements. Note that aircraft profiles are not assimilated in CT2015, so aircraft data are independent of the CT2015 data assimilation. Figure 7b shows monthly partial columns of $\Delta XCO_2$ calculated from CT2015, which demonstrate good agreement with results from measurements. Only small seasonal biases exist in CT2015, with high bias occurring mostly in spring and early summer and low bias in September and October (Fig. S4). The overall differences of monthly partial column $\Delta XCO_2$ (CT2015 - measurements) mainly fall in the range of -0.64 ppm (5th percentile) to 0.84 ppm (95th percentile) with a mean difference of 0.13 ppm. These differences are of similar magnitude to the uncertainties of partial column $\Delta XCO_2$ calculated from the measurements (Fig. S5). It is clear that CT2015 captures the long-term mean variations of both phase and amplitude of partial column $XCO_2$ reasonably well when compared with well-calibrated measurements across North America.
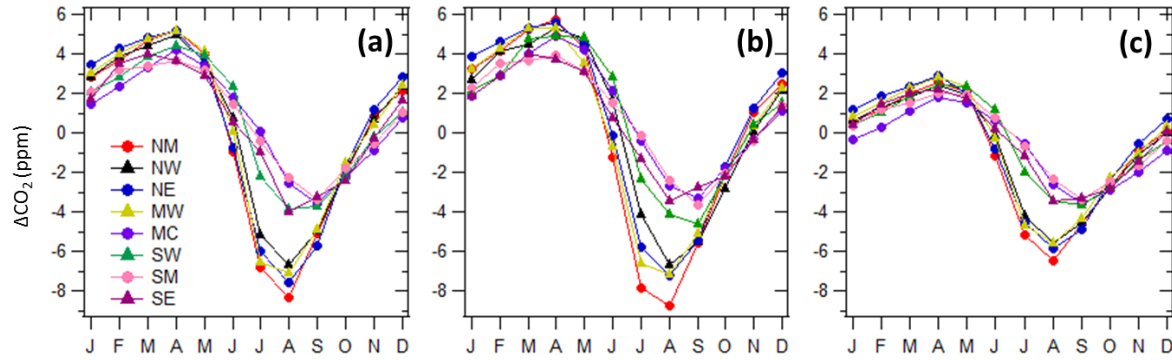
**Fig. 7**. (a). Partial column $\Delta XCO_2$ calculated from aircraft and tower data; (b). Partial column $\Delta XCO_2$ calculated from CT2015; (c). Total column $\Delta XCO_2$ calculated from aircraft and tower data and including the top layer data from CT2015.

Total column $\Delta XCO_2$ is presented in Fig. 7c. In regions NW, NM, NE, and MW, seasonal variations of total column $\Delta XCO_2$ are very similar in both phase and amplitude (8-9 ppm peak to valley). For SW, SM, SE, and MC, amplitudes are ~5.5 ppm. The smallest spatial gradients occur during May and October, which result in maximum differences among all regions of only 0.9 and 0.7 ppm, respectively. The largest spatial gradients occur during June, July and August, which result in maximum differences of 2.4, 4.5, and 4.1 ppm, respectively. It is interesting that the deepest seasonal drawdown is seen in region NM, not in region MW that encompasses the very intensive

agricultural activities in the U.S. mid-west, which suggest the possibility of strong upwind influence in the NM region. Transported signals have significant influences on total column $CO_2$. The summer total column $\Delta XCO_2$, represented by the June to August average from CT2015, has a magnitude that is similar to observations with differences no more than 1 ppm (Fig. 8). Based on the seasonal patterns of total column $\Delta XCO_2$ (Fig. 7c) and the summer column $\Delta XCO_2$ (Fig. 8), we can separate the eight regions into two groups. The group with NW, NM, NE, and MW, has ~3 ppm stronger drawdown (larger amplitude) than the group with SW, SM, SE, and MC. For winter total column $\Delta XCO_2$ (December to February average), the maximum spatial difference is only 1.6 ppm, with the highest total column $\Delta XCO_2$ of 1.2 ppm in NE and the lowest value of -0.3 ppm in MC.
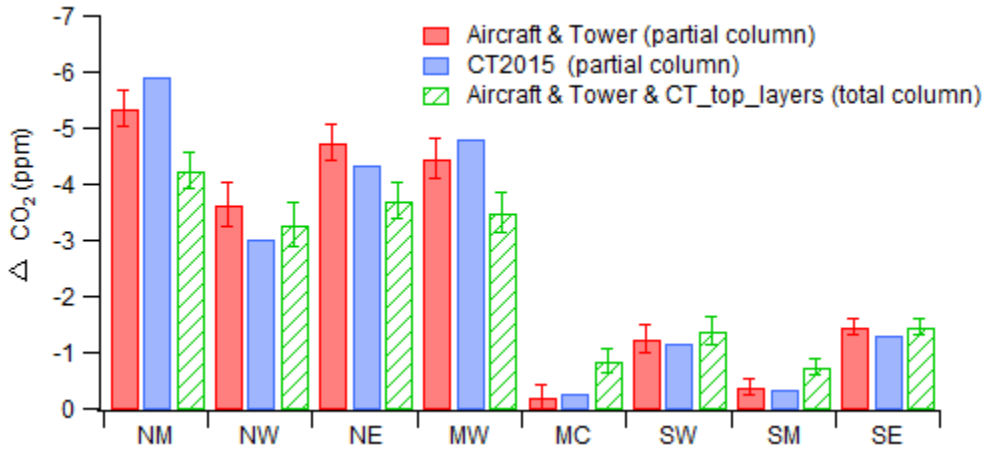
**Fig. 8**. Long-term mean (2004-2014) June to August partial and total column $\Delta XCO_2$. Error bars represent one standard deviation from the bootstrap uncertainty calculation (see Sect. 2.3).

**3.4 Influence of large scale circulation**

Figure 9 shows long-term mean summer column $\Delta XCO_2$ calculated from CT2015, together with full column $\Delta XCO_2$ from individual aircraft sites. Note that some aircraft sites have less than 11 years of data that CT2015 shows in Fig. 9, only aircraft sites with more than 6 years of data are presented, the actual values are provided in Table S2. The fact that total column $\Delta XCO_2$ from CT2015 agrees well with aircraft sites supports the performance of CT2015 on a long-term average basis. The observations show a similar summer spatial pattern, with lower column $\Delta XCO_2$ in the north and northeast regions and higher column $\Delta XCO_2$ in the south and southwest regions (Fig. 9a). Scattered hot spots of high column $\Delta XCO_2$ associated with surface emissions from megacities, or cold spots associated with strong local uptake, are not or just barely visible in the long-term average column $\Delta XCO_2$ map at 1°x1° resolution. Instead, the wave-like pattern of column $\Delta XCO_2$ over North America reflects the average large scale circulation. To support our hypothesis on the influence of large scale circulation, we analyze the long term mean wind pattern over North America. We can see that air masses from northwest of the continent bring in low average column $\Delta XCO_2$, while air masses from the south (mainly the subtropical Pacific Ocean and the Gulf of

Mexico) bring in high column $\Delta XCO_2$ (Fig. 9b). The zonal gradients over the continent, especially north of 40° N, also reflect long-term average wind patterns; southwest wind corresponds to higher column $\Delta XCO_2$ over the western part of the continent until the wind direction shifts to west-northwest over the eastern part of the continent. This wind pattern matches well with the geographic division of the over/under -3 ppm areas colored in green/blue in the column $\Delta XCO_2$ map (Fig. 9b). Figure 9c and 9d shows partial column averages for free troposphere (800-330 hPa) and lower troposphere (below 800 hPa), respectively. The free troposphere spatial gradient also demonstrates a wave-like pattern. A previous study on the total column $CO_2$ from ground based Total Carbon Column Observation Network (TCCON) found strong correlation between the mid-latitude column $CO_2$ and synoptic-scale variation of potential temperature ($\theta$, at 700 hPa ), a dynamic tracer for adiabatic air transport (Keppel-Aleks et al., 2012). Thus they also propose that the variations in column $CO_2$ are mainly driven by large-scale flux and transport. Analysis of the interannual variability of the seasonal cycle amplitudes of column $CO_2$ in North Hemisphere has also found significant contribution of large-scale circulations to the north-south gradient (Wunch et al., 2013).

The strong drawdown over northeast North America in summer is a consequence of long-range transport of low $CO_2$ from northeast Eurasia, in addition to regional terrestrial uptake. Sweeney et al. (2015) notes well-mixed vertical profiles (up to 8 km) of $CO_2$, CO, $CH_4$, $N_2O$, and $SF_6$ from THD, ESP and PFA (Poker Flat, Alaska; 65.07°, -147.29°) sites and suggests that air coming across the Pacific was strongly influenced by Asian surface fluxes before being vertically homogenized as it passed over the Pacific Ocean. This well-mixed air forms an important boundary condition in the column $CO_2$ of air coming into the North American continent. This was best illustrated at sites like PFA where the summertime minimum in $CO_2$ significantly preceded maximum ecosystem uptake of $CO_2$, implying significant influence of transported air from lower latitude regions from Asia. We further conduct an experiment using Carbon Tracker to investigate the importance of this effect. A control run and a "masked run" are conducted for 2010-2012, in which the Eurasian boreal flux is turned on/off. The MLO $CO_2$ trend from each model scenario is used as reference background and thus removed before total column $\Delta XCO_2$ calculation. Figure 10 shows the results for 2012 summer, which is an average summer when compared with the 2004-2014 mean pattern (Fig. 9 and Fig. 11). The maximum north-south difference reduces to ~2.5 ppm after we turn off the Eurasian boreal flux, compared with ~5 ppm from the control run. In both control and masked scenarios, the free troposphere partial $\Delta XCO_2$ demonstrates similar spatial patterns as for total column $\Delta XCO_2$ (Fig. S6). This result combined with results from Sweeney et al. (2015) demonstrates that the transport of low $CO_2$ resulting from large summertime Eurasian boreal uptake has a large contribution on the overall summer total column $CO_2$ decrease in North America.
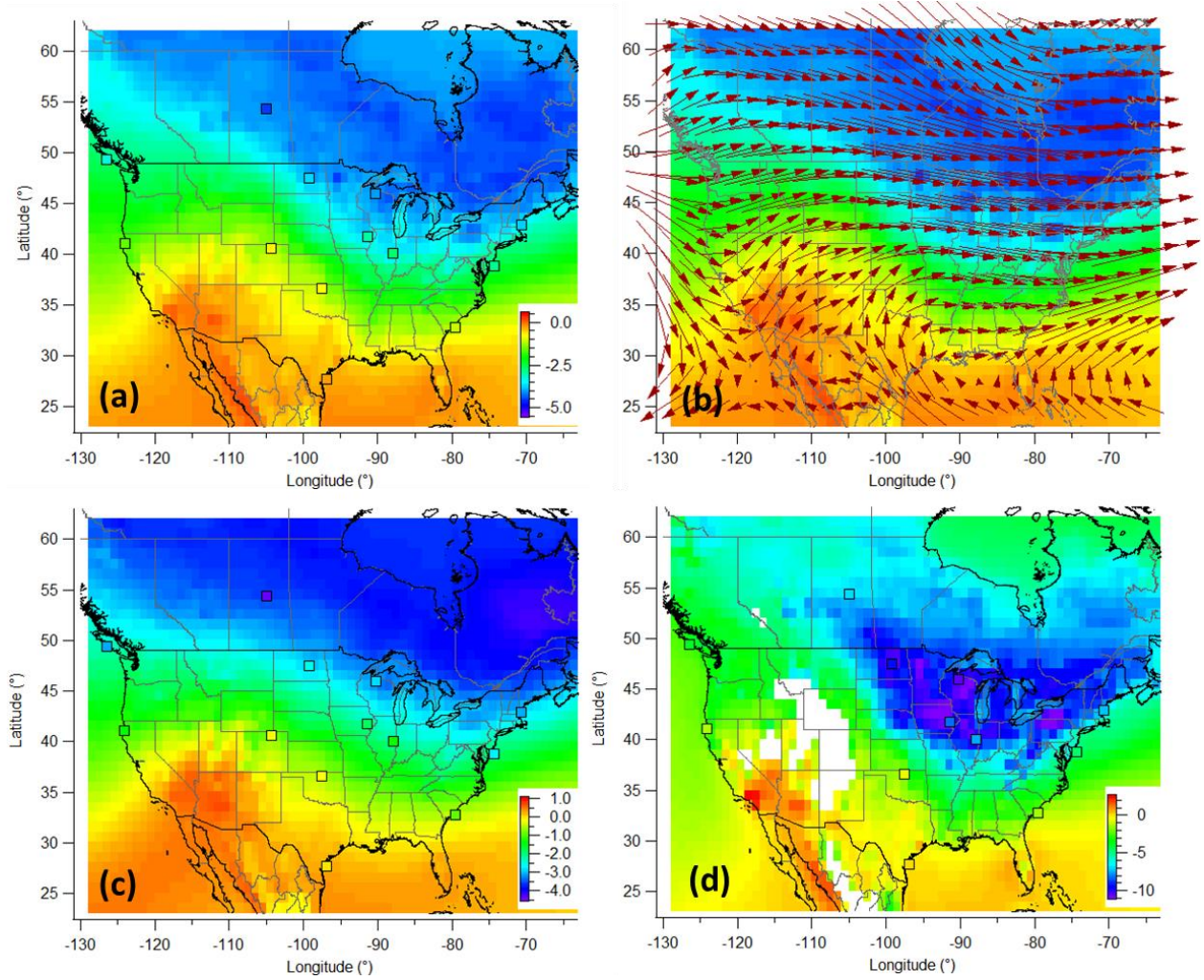
**Fig. 9**. Long-term mean (2004-2014) June-August total column $\Delta XCO_2$ from CT2015 in $1° \times 1°$ spatial resolution with total column $\Delta XCO_2$ for 13 individual aircraft sites in squares (a), and CT2015 column $\Delta XCO_2$ overlaid with pressure-weighted (1000 hPa to 500 hPa) mean wind vectors for the same period (b). (c) and (d) are similar as (a), except for free troposphere (800 to 330 hPa) and lower troposphere (below 800 hPa), respectively. Note the different color scales.
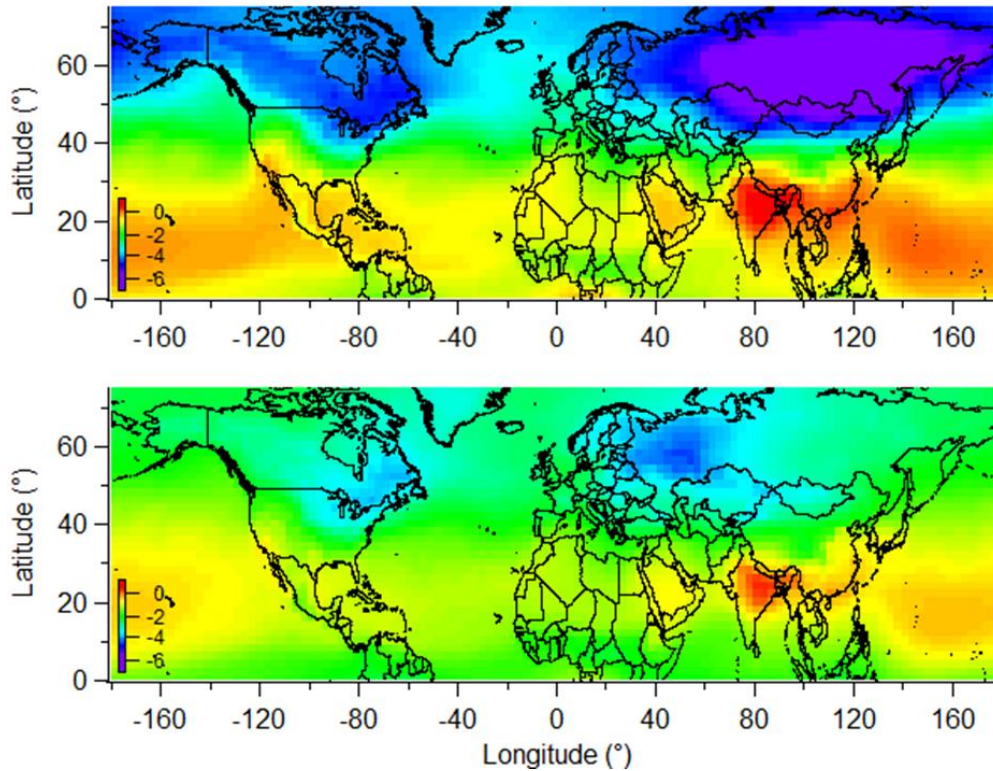
**Fig. 10**. Total column ΔXCO₂ from Carbon Tracker control (top panel) and masked (bottom panel, Eurasian boreal flux is masked) runs for 2012 June-August (3° × 2° spatial resolution). MLO trend from each individual scenario is removed before the ΔXCO₂ calculation. Same color scale is used as in Fig. 9a. Partial column ΔXCO₂ patterns for free troposphere (800 to 330 hPa) and lower troposphere (below 800 hPa) are provided in SI.

### 3.5 A comparison with apparent gradients over Europe

Figure 11 shows the climatological June - August mean modeled global column ΔXCO₂ map in 3° × 2° spatial resolution, which presents smooth wave-like patterns. Reuter et al. (2014) use SCIAMACHY and GOSAT satellite retrievals of column CO₂ and inverse modelling to infer a very large net CO₂ uptake flux over European region. Column ΔXCO₂ from CT2015 (Fig. 11) exhibits a drastically different summer spatial pattern over Europe compared with the eight year mean (2003-2010) June through August satellite retrievals presented by Reuter et al. (2014, their Fig. 2a). The spatial gradient from CT2015 results in a maximum 3-4 ppm difference and a gradual pattern, instead of as much as 6 ppm from satellite retrievals. There is no sign of XCO₂ hot spots from surface emissions or removals in the CT2015 spatial pattern over Europe (Fig. 11), in contrast to several hot spots that are apparent from the 8-year averaged SCIAMACHY satellite retrievals over Ireland, U.K., Belgium, Netherland, north of Germany, and south of Sweden, and low spots over the Ukraine and Kazakhstan (Reuter et al., 2014). This SCIAMACHY retrieval pattern contradicts our understanding of the significant influence of large-scale transport on column ΔXCO₂. Although the NOAA/ESRL CT2015 (https://www.esrl.noaa.gov/gmd/ccgg/carbontracker/CT2015/) assimilates fewer observations over Europe than Carbon Tracker Europe (http://www.carbontracker.eu/), both

models produced similar fluxes over the European region (see both websites for detailed fluxes). The $3^o \times 2^o$ grid from CT2015 is not likely responsible for a much smoother pattern for Carbon Tracker, compared with the $2^o \times 2^o$ grid from satellite retrievals (Reuter et al., 2014) . The North America region on the $3^0 \times 2^0$ grid in Fig. 11 shows similar pattern as the $1^o \times 1^o$ grid in Fig. 9, with similar spatial difference of ~ 5 ppm. A smoother spatial distribution should be expected in Europe for the long-term mean column $XCO_2$ (Fig. 11) due to the influences of dominating west and southwest winds in summer. We have also evaluated the importance of sampling bias by sampling CT2015 at the same latitude/longitude/hour (within 1 hour) as in SCIAMACHY BESD (v02.00.08) data (Reuter et al., 2011). The 8-year mean pattern shows much smaller gradients (3-4 ppm maximum) without significant hot/cold spots at the locations of SCIAMACHY (Fig. S7). Although sampling biases contribute to the unphysical column $XCO_2$ spatial pattern from SCIAMACHY, they cannot explain the large gradients. When we compare CT2015 directly with SCIAMCHY BESD data, we find up to ~3 ppm differences over North America and Europe (Fig. S8). Since CT2015 compares well with calibrated data over North America, we are deeply skeptical about any sources/sinks inferred from the SCIAMACHY BESD data. A recent study (Feng et al., 2016) using inverse modeling suggests that satellite retrievals outside the immediate European region and a small bias of only 0.5 ppm were sufficient to produce the apparent large carbon sink in the study of Reuter et al. (2014). This is expected from elementary mass balance considerations as in Sec.1 above. Spatial gradients are the fundamental signals to infer regional fluxes. Since spatial gradients from CT2015 are realistic, boreal fluxes inferred by CT2015, should be more trustworthy than fluxes estimated based on unrealistic spatial pattern. The European carbon sink is still inconclusive; the discrepancies among different methods and results are further discussed by Reuter et al. (2017).
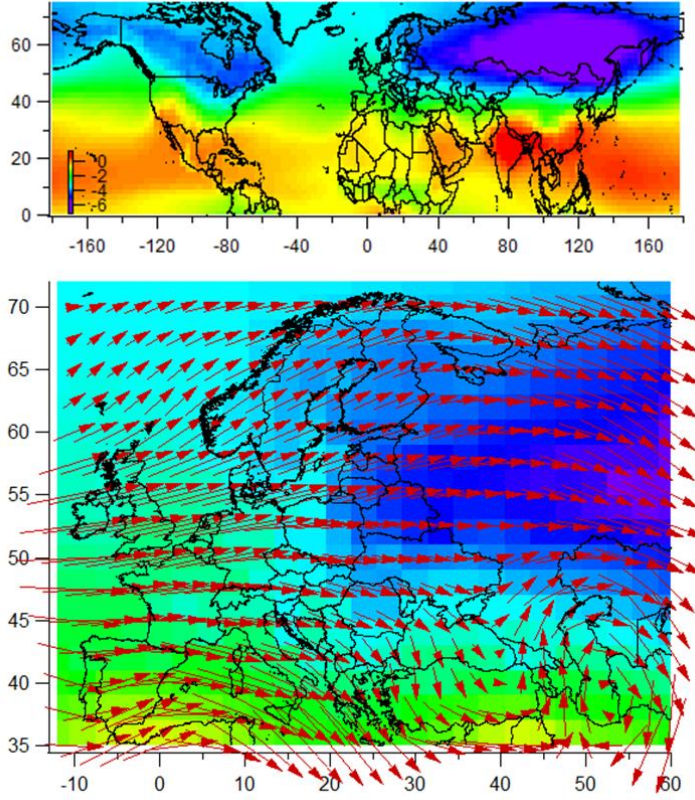
**Fig. 11**. Long-term mean (2004-2014) June - August total column $\Delta XCO_2$ from CT2015 (top panel) in $3° \times 2°$ spatial resolution, and detail for Europe overlaid with pressure-weighted (1000 hPa to 500 hPa) mean wind vectors for the same period (bottom panel). The color scale is the same as in Fig. 9a, which is scaled to reflect 6 ppm difference of $XCO_2$ to compare with satellite retrievals from Reuter et al. (their Fig. 2a, 2014).

## 4 Conclusion

Aircraft and tall tower measurements from the NOAA GGGRN provide detailed information describing the long-term average temporal and spatial variations of $CO_2$ in the PBL and the free troposphere. These data provide valuable constraints for evaluating model simulations and satellite retrievals. Seasonal cycle peak-to-peak amplitudes of $CO_2$ are largest below 2 km, where those maximum values are about twice those in the vertical layers above, indicating that most of the information on surface sources and sinks resides in the continental PBL. Large spatial gradients of $CO_2$ over North America are observed below 2 km during summer (with maximum difference of ~15.5 ppm between MW and SM), while higher altitude data (above 2 km) have much smaller contributions to spatial gradients, with a maximum difference of 4 ppm. The spatial differences of $CO_2$ in the upper troposphere and above (330 hPa to 0 hPa) are less than 0.5 ppm, according to CT2015. Comparison with Aircore measurements shows CT2015 performs well simulating upper tropospheric and lower stratospheric patterns.

Our long-term mean vertical profiles show that tower data agree well with aircraft data at similar vertical levels. Partial column $\Delta XCO_2$ was calculated from the long-term mean vertical profiles. By comparing the partial column

$\Delta XCO_2$ from measurements with those from CT2015, we verify that CT2015 captures the long-term mean patterns of both phase and amplitude of partial $\Delta XCO_2$.

Large spatial gradients of $\Delta XCO_2$ only appeared in summer, during which time the north and northeast regions had ~3 ppm stronger drawdowns than the south and southwest regions. Scattered hot spots of high column $\Delta XCO_2$ associated with surface emissions from megacities, or cold spots associated with strong local uptake, are not or just barely visible in the long-term average column $\Delta XCO_2$. Instead, the wave-like pattern of column $\Delta XCO_2$ over North America matches well with the average large scale circulation. A CarbonTracker experiment to investigate the impact of Eurasian long-range transport suggests that the large summer time Eurasian boreal flux alone contributes about half of the north-south column $\Delta XCO_2$ gradient across North America. Considering the transported signals from other upwind regions, including northern Canada, we expect that the transported signals have the overall largest contribution to the total column $\Delta XCO_2$ spatial gradient.

## Author contributions

Xin Lan was responsible for study design, data analysis, and manuscript writing. Pieter Tans was responsible for study design, data analysis, and manuscript improvement. Colm Sweeney and Arlyn Andrews provided measurement data and improved manuscript. Andrew Jacobson provided modelled data and improved manuscript. Edward Dlugokencky analyzed measurements and ensured data quality, and improved manuscript. Jonathan Kofler conducted tower measurements and improved manuscript. Molly Crotwell, Patricia Lang, and Sonja Wolter analyzed measurements and ensured data quality. Kirk Thoning provided data smoothing method.

## Acknowledgements

We especially thank John Mund for extracting NARR meteorological variables for our measurements. This research was supported by a fellowship from the National Research Council Research Associateship Programs.

## References

Andrews, A. E., Kofler, J. D., Trudeau, M. E., Williams, J. C., Neff, D. H., Masarie, K. A., Chao, D. Y., Kitzis, D. R., Novelli, P. C., Zhao, C. L., Dlugokencky, E. J., Lang, P. M., Crotwell, M. J., Fischer, M. L., Parker, M. J., Lee, J. T., Baumann, D. D., Desai, A. R., Stanier, C. O., De Wekker, S. F. J., Wolfe, D. E., Munger, J. W. and Tans, P. P.: CO2, CO, and CH4 measurements from tall towers in the NOAA Earth System Research Laboratory's Global Greenhouse Gas Reference Network: instrumentation, uncertainty analysis, and recommendations for future high-accuracy greenhouse gas monitoring efforts, Atmos. Meas. Tech., 7, 647-687, 2014.

Banta, R. M., Senff, C. J., Nielsen-Gammon, J., Darby, L. S., Ryerson, T. B., Alvarez, R. J., Sandberg, S. R., Williams, E. J. and Trainer, M.: A bad air day in Houston', B. Am. Meteorol. Soc., 86, 657, DOI: http://dx.doi.org/10.1175/BAMS-86-5-657, 2005.

Biraud, S. C., Torn, M. S., Smith, J. R., Sweeney, C., Riley, W. J. and Tans, P. P.:A multi-year record of airborne $CO_2$ observations in the US Southern Great Plains, Atmos. Meas. Tech., 6, 751-763, 2013.

Buchwitz, M., Reuter, M., Bovensmann, H., Pillai, D., Heymann, J., Schneising, O., Rozanov, V., Krings, T., Burrows, J. P., Boesch, H., Gerbig, C., Meijer, Y. and Loscher, A. : Carbon Monitoring Satellite (CarbonSat): assessment of atmospheric $CO_2$ and $CH_4$ retrieval errors by error parameterization, Atmos. Meas. Tech., 6, 3477-3500, 2013.

Chevallier, F., Breon, F. M. and Rayner, P. J.: Contribution of the Orbiting Carbon Observatory to the estimation of $CO_2$ sources and sinks: Theoretical study in a variational data assimilation framework, J. Geophys. Res. Atmos., 112, D09307, doi:10.1029/2006JD007375, 2007.

Choi, Y. H., Vay, S. A., Vadrevu, K. P., Soja, A. J., Woo, J. H., Nolf, S. R., Sachse, G. W., Diskin, G. S., Blake, D. R., Blake, N. J., Singh, H. B., Avery, M. A., Fried, A., Pfister, L. and Fuelberg, H. E.: Characteristics of the atmospheric $CO_2$ signal as observed over the conterminous United States during INTEX-NA, J. Geophys. Res. Atmos., 113, D07301, doi:10.1029/2007JD008899, 2008.

Ciais, P., Rayner, P., Chevallier, F., Bousquet, P., Logan, M., Peylin, P. and Ramonet, M.: Atmospheric inversions for estimating $CO_2$ fluxes: methods and perspectives, Climatic Change, 103, 69-92, 2010.

Conway, T. J., Tans, P. P., Waterman, L. S. and Thoning, K. W.: Evidence for interannual variability of the carbon-cycle from the national-oceanic-and-atmospheric-administration climate-monitoring-and-diagnostics-laboratory global-air-sampling-network, J. Geophys. Res. Atmos., 99, 22831-22855, 1994.

Crevoisier, C., Sweeney, C., Gloor, M., Sarmiento, J. L. and Tans, P. P.: Regional US carbon sinks from three-dimensional atmospheric $CO_2$ sampling, Proc. Natl. Acad. Sci. U. S. A., 107, 18348-18353, 2010.

Crisp, D., Fisher, B. M., O'Dell, C., Frankenberg, C., Basilio, R., Bosch, H., Brown, L. R., Castano, R., Connor, B., Deutscher, ¨ N. M., Eldering, A., Griffith, D., Gunson, M., Kuze, A., Mandrake, L., McDuffie, J., Messerschmidt, J., Miller, C. E., Morino, I., Natraj, V., Notholt, J., O'Brien, D. M., Oyafuso, F., Polonsky, I., Robinson, J., Salawitch, R., Sherlock, V., Smyth, M., Suto, H., Taylor, T. E., Thompson, D. R., Wennberg, P. O., Wunch, D., and Yung, Y. L.: The ACOS $CO_2$ retrieval algorithm – Part II: Global $XCO_2$ data characterization, Atmos. Meas. Tech., 5, 687–707, doi:10.5194/amt-5-687-2012, 2012.

Dee, D. P., Uppala, S. M., Simmons, A. J., Berrisford, P., Poli, P., Kobayashi, S., Andrae, U., Balmaseda, M. A., Balsamo, G., Bauer, P., Bechtold, P., Beljaars, A. C. M., van de Berg, L., Bidlot, J., Bormann, N., Delsol, C., Dragani, R., Fuentes, M., Geer, A. J., Haimberger, L., Healy, S. B., Hersbach, H., Holm, E. V., Isaksen, L., Kallberg, P., Kohler, M., Matricardi, M., McNally, A. P., Monge-Sanz, B. M., Morcrette, J. J., Park, B. K., Peubey, C., de Rosnay, P., Tavolato, C., Thepaut, J. N. and Vitart, F.: The ERA-Interim reanalysis: configuration and performance of the data assimilation system, Q.J.R. Meteorol. Soc., 137, 553-597, 2011.

Denning, A. S., Takahashi, T., and Friedlingstein, P.: Can a strong atmospheric $CO_2$ rectifier effect be reconciled with a "reasonable" carbon budget?, Tellus B, 51, 249–253, 1999.

Feng, L., Palmer, P. I., Parker, R. J., Deutscher, N. M., Feist, D. G., Kivi, R., Morino, I. and Sussmann, R.: Estimates of European uptake of $CO_2$ inferred from GOSAT X-$CO_2$ retrievals: sensitivity to measurement bias inside and outside Europe, Atmos. Chem. Phys., 16, 1289-1302, 2016.

Frankenberg, C., Kulawik, S. S., Wofsy, S., Chevallier, F., Daube, B., Kort, E. A., O'Dell, C., Olsen, E. T., and Osterman, G.: Using airborne HIAPER Pole-to-Pole Observations (HIPPO) to evaluate model and remote sensing estimates of atmospheric carbon dioxide, Atmos. Chem. Phys., , 16, 7867−7878, 2016. doi:10.5194/acp-16-7867-2016, 2016.

Gerbig, C., Lin, J. C., Wofsy, S. C., Daube, B. C., Andrews, A. E., Stephens, B. B., Bakwin, P. S. and Grainger, C. A.: Toward constraining regional-scale fluxes of CO2 with atmospheric observations over a continent: 1. Observed spatial variability from airborne platforms J. Geophys. Res. Atmos., 108, doi:10.1029/2002JD003018, 2003.

Chevallier, F., Palmer, P. I., Feng, L., Boesch, H., O'Dell, C. W., and Bousquet, P.: Towards robust and consistent regional $CO_2$ flux estimates from in situ and space-borne measurements of atmospheric $CO_2$, Geophys. Res. Lett., 41, 1065−1070, doi:10.1002/2013GL058772, 2014.

Gourdji, S. M., Mueller, K. L., Yadav, V., Huntzinger, D. N., Andrews, A. E., Trudeau, M., Petron, G., Nehrkorn, T., Eluszkiewicz, J., Henderson, J., Wen, D., Lin, J., Fischer, M., Sweeney, C. and Michalak, A. M.: North American CO2 exchange: inter-comparison of modeled estimates with results from a fine-scale atmospheric inversion, Biogeosci., 9, 457-475, 2012

Gurney, K. R., Law, R. M., Denning, A. S., Rayner, P. J., Baker, D., Bousquet, P., Bruhwiler, L., Chen, Y. H., Ciais, P., Fan, S., Fung, I. Y., Gloor, M., Heimann, M., Higuchi, K., John, J., Maki, T., Maksyutov, S., Masarie, K., Peylin, P., Prather, M., Pak, B. C., Randerson, J., Sarmiento, J., Taguchi, S., Takahashi, T. and Yuen, C. W.: Towards robust regional estimates of CO2 sources and sinks using atmospheric transport models, Nature, 415(6872), 626-630, 2002.

Gurney, K. R., Law, R. M., Denning, A. S., Rayner, P. J., Pak, B. C., Baker, D., Bousquet, P., Bruhwiler, L., Chen, Y. H., Ciais, P., Fung, I. Y., Heimann, M., John, J., Maki, T., Maksyutov, S., Peylin, P., Prather, M. and Taguchi, S.: Transcom 3 inversion intercomparison: Model mean results for the estimation of seasonal carbon sources and sinks, Global Biogeochem. Cycles, 18, GB1010, doi:10.1029/2003GB002111, 2004.

Houweling, S., Breon, F. M., Aben, I., Rodenbeck, C., Gloor, M., Heimann, M. and Ciais, P.: Inverse modeling of CO2 sources and sinks using satellite data: a synthetic inter-comparison of measurement techniques and their performance as a function of space and time, Atmos. Chem. Phys., 4, 523-538, 2004.

Inoue, M., Morino, I., Uchino, O., Miyamoto, Y., Yoshida, Y., Yokota, T., Machida, T., Sawa, Y., Matsueda, H., Sweeney, C., Tans, P. P., Andrews, A. E., Biraud, S. C., Tanaka, T., Kawakami, S. and Patra, P. K.: Validation of XCO2 derived from SWIR spectra of GOSAT TANSO-FTS with aircraft measurement data, Atmos. Chem. Phys., 13, 9771-9788, 2013.

Inoue, M., Morino, I., Uchino, O., Nakatsuru, T., Yoshida, Y., Yokota, T., Wunch, D., Wennberg, P. O., Roehl, C. M., Griffith, D. W. T., Velazco, V. A., Deutscher, N. M., Warneke, T., Notholt, J., Robinson, J., Sherlock, V., Hase, F., Blumenstock, T., Rettinger, M., Sussmann, R., Kyrö, E., Kivi, R., Shiomi, K., Kawakami, S., De Mazière, M., Arnold, S. G., Feist, D. G., Barrow, E. A., Barney, J., Dubey, M., Schneider, M., Iraci, L., Podolske, J. R., Hillyard, P., Machida, T., Sawa, Y., Tsuboi, K., Matsueda, H., Sweeney, C., Tans, P. P., Andrews, A. E., Biraud, S. C., Fukuyama, Y., Pittman, J. V., Kort, E. A., and Tanaka, T.: Bias corrections of

GOSAT SWIR XCO2 and XCH4 with TCCON data and their evaluation using aircraft measurement data, Atmos. Meas. Tech. 9, 3491–3512, 2016, doi:10.5194/amt-9-3491-2016.

Karion, A., Sweeney, C., Tans, P., and Newberger, T.: AirCore: An Innovative Atmospheric Sampling System, J. Atmos. Ocean. Tech., 27, 1839–1853, doi:10.1175/2010JTECHA1448.1, 2010.

Karion, A., C. Sweeney, S. Wolter, T. Newberger, H. Chen, A. Andrews, J. Kofler, D. Neff, and P. Tans (2013), Long-term greenhouse gas measurements from aircraft, Atmos. Meas. Tech., 6(3), 511–526, doi:10.5194/amt-6-511-2013.

Keeling, C. D. and Rakestraw, N. W.: The concentration of carbon dioxide in the atmosphere, J. Geophys. Res., 65, 2502-2502, 1960.

Keppel-Aleks, G., Wennberg, P. O., Washenfelder, R. A., Wunch, D., Schneider, T., Toon, G. C., Andres, R. J., Blavier, J.-F., Connor, B., Davis, K. J., Desai, A. R., Messerschmidt, J., Notholt, J., Roehl, C. M., Sherlock, V., Stephens, B. B., Vay, S. A., and Wofsy, S. C.: The imprint of surface fluxes and transport on variations in total column carbon dioxide, Biogeosci., 9, 875– 891, doi:10.5194/bg-9-875-2012, 2012.

Kulawik, S. S., Worden, J. R., Wofsy, S. C., Biraud, S. C., Nassar, R., Jones, D. B. A., Olsen, E. T., Jimenez, R., Park, S., Santoni, G. W., Daube, B. C., Pittman, J. V., Stephens, B. B., Kort, E. A., Osterman, G. B. and Team, T. E. S.: Comparison of improved Aura Tropospheric Emission Spectrometer CO2 with HIPPO and SGP aircraft profile measurements, Atmos. Chem. Phys., 13, 3205-3225, 2013.

Lauvaux, T., Schuh, A. E., Uliasz, M., Richardson, S., Miles, N., Andrews, A. E., Sweeney, C., Diaz, L. I., Martins, D., Shepson, P. B. and Davis, K. J.: Constraining the CO2 budget of the corn belt: exploring uncertainties from the assumptions in a mesoscale inverse system, Atmos. Chem. Phys., 12, 337-354, 2012.

Machida, T., Kita, K., Kondo, Y., Blake, D., Kawakami, S., Inoue, G. and Ogawa, T. : Vertical and meridional distributions of the atmospheric CO2 mixing ratio between northern midlatitudes and southern subtropics, J. Geophys. Res. Atmos., 108(D3), 8401, doi:10.1029/2001JD000910, 2002.

Machida, T., Matsueda, H., Sawa, Y., Nakagawa, Y., Hirotani, K., Kondo, N., Goto, K., Nakazawa, T., Ishikawa, K. and Ogawa, T.: Worldwide Measurements of Atmospheric CO2 and Other Trace Gas Species Using Commercial Airlines, J. Atmos. Ocean. Tech., 25(10), 1744-1754, 2008.

Mesinger, F., DiMego, G., Kalnay, E., Mitchell, K., Shafran, P. C., Ebisuzaki, W., Jovic, D., Woollen, J., Rogers, E., Berbery, E. H., Ek, M. B., Fan, Y., Grumbine, R., Higgins, W., Li, H., Lin, Y., Manikin, G., Parrish, D., and Shi, W.: North American regional reanalysis, B. Am. Meteorol. Soc., 87, 343–360, doi:10.1175/BAMS-87-3-343, 2006.

Messerschmidt, J., Geibel, M. C., Blumenstock, T., Chen, H., Deutscher, N. M., Engel, A., Feist, D. G., Gerbig, C., Gisi, M., Hase, F., Katrynski, K., Kolle, O., Lavric, J. V., Notholt, J., Palm, M., Ramonet, M., Rettinger, M., Schmidt, M., Sussmann, R., Toon, G. C., Truong, F., Warneke, T., Wennberg, P. O., Wunch, D. and Xueref-Remy, I.: Calibration of TCCON column-averaged CO2: the first aircraft campaign over European TCCON sites, Atmos. Chem. Phys., 11(21), 10765-10777, 2011.

Miller, C. E., Crisp, D., DeCola, P. L., Olsen, S. C., Randerson, J. T., Michalak, A. M., Alkhaled, A., Rayner, P., Jacob, D. J., Suntharalingam, P., Jones, D. B. A., Denning, A. S., Nicholls, M. E., Doney, S. C., Pawson, S.,

Boesch, H., Connor, B. J., Fung, I. Y., O'Brien, D., Salawitch, R. J., Sander, S. P., Sen, B., Tans, P., Toon, G. C., Wennberg, P. O., Wofsy, S. C., Yung, Y. L. and Law, R. M.: Precision requirements for space-based X-CO2 data, J. Geophys. Res. Atmos., 112, D10314, doi:10.1029/2006JD007659, 2007.

Miller, J. B., Lehman, S. J., Montzka, S. A., Sweeney, C., Miller,B. R., Karion, A., Wolak, C., Dlugokencky, J., Southon, J., Turnbull, J. C., and Tans, P. P.: Linking emissions of fossil fuel CO2 and other anthropogenic trace gases using atmospheric 14CO2, J. Geophys. Res., 117, D08302, doi:10.1029/2011JD017048, 2012.

Miller, S. T. K., Keim, B. D., Talbot, R. W. and Mao, H.: Sea breeze: Structure, forecasting, and impacts, Rev. Geophys., 41, 1011, doi:10.1029/2003RG000124, 2003.

Miyamoto, Y., Inoue, M., Morino, I., Uchino, O., Yokota, T., Machida, T., Sawa, Y., Matsueda, H., Sweeney, C., Tans, P. P., Andrews, A. E. and Patra, P. K.: Atmospheric column-averaged mole fractions of carbon dioxide at 53 aircraft measurement sites, Atmos. Chem. Phys., 13(10), 5265-5275, 2013.

Peters, W., Jacobson, A. R., Sweeney, C., Andrews, A. E., Conway, T. J., Masarie, K., Miller, J. B., Bruhwiler, L. M. P., Petron, G., Hirsch, A. I., Worthy, D. E. J., van der Werf, G. R., Randerson, J. T., Wennberg, P. O., Krol, M. C. and Tans, P. P.: An atmospheric perspective on North American carbon dioxide exchange: CarbonTracker, Proc. Natl. Acad. Sci. U. S. A., 104(48), 18925-18930, 2007.

Ramonet, M., Ciais, P., Nepomniachii, I., Sidorov, K., Neubert, R. E. M., Langendorfer, U., Picard, D., Kazan, V., Biraud, S., Gusti, M., Kolle, O., Schulze, E. D. and Lloyd, J.: Three years of aircraft-based trace gas measurements over the Fyodorovskoye southern taiga forest, 300 km north-west of Moscow, Tellus B-Chem. Phys. Meteor., 54(5), 713-734, 2002.

Reuter, M., Bovensmann, H., Buchwitz, M., Burrows, J. P., Connor, B. J., Deutscher, N. M., Griffith, D. W. T., Heymann, J., Keppel-Aleks, G., Messerschmidt, J., Notholt, J., Petri, C., Robinson, J., Schneising, O., Sherlock, V., Velazco, V., Warneke, T., Wennberg, P. O. and Wunch, D.: Retrieval of atmospheric CO2 with enhanced accuracy and precision from SCIAMACHY: Validation with FTS measurements and comparison with model results, J. Geophys. Res. Atmos., 116, 2011.

Reuter, M., Buchwitz, M., Hilker, M., Heymann, J., Schneising, O., Pillai, D., Bovensmann, H., Burrows, J. P., Bosch, H., Parker, R., Butz, A., Hasekamp, O., O'Dell, C. W., Yoshida, Y., Gerbig, C., Nehrkorn, T., Deutscher, N. M., Warneke, T., Notholt, J., Hase, F., Kivi, R., Sussmann, R., Machida, T., Matsueda, H. and Sawa, Y.: Satellite-inferred European carbon sink larger than expected, Atmos. Chem. Phys., 14(24), 13739-13753, 2014.

Reuter, M., Buchwitz, M., Hilker, M., Heymann, J., Bovensmann, H., Burrows, J. P., Houweling, S., Liu, Y. Y., Nassar, F., Chevallier, F., Cias, P., Marshall, J., and Reichstein, M.: How much CO2 is taken up by the European terrestrial biosphere? Bull. Am. Meteor. Soc., 98, 665–671, doi:10.1175/BAMS-D-15-00310.1, 2017.

Saitoh, N., Kimoto, S., Sugimura, R., Imasu, R., Kawakami, S., Shiomi, K., Kuze, A., Machida, T., Sawa, Y. and Matsueda, H.: Algorithm update of the GOSAT/TANSO-FTS thermal infrared CO2 product (version 1) and validation of the UTLS CO2 data using CONTRAIL measurements, Atmos. Meas. Tech., 9(5), 2119-2134, 2016.

Stephens, B. B., Gurney, K. R., Tans, P. P., Sweeney, C., Peters, W., Bruhwiler, L., Ciais, P., Ramonet, M., Bousquet, P., Nakazawa, T., Aoki, S., Machida, T., Inoue, G., Vinnichenko, N., Lloyd, J., Jordan, A., Heimann, M., Shibistova, O., Langenfelds, R. L., Steele, L. P., Francey, R. J. and Denning, A. S.: Weak northern and strong tropical land carbon uptake from vertical profiles of atmospheric CO(2), Science, 316(5832), 1732-1735, 2007.

Sweeney, C., Karion, A., Wolter, S., Newberger, T., Guenther, D., Higgs, J. A., Andrews, A. E., Lang, P. M., Neff, D., Dlugokencky, E., Miller, J. B., Montzka, S. A., Miller, B. R., Masarie, K. A., Biraud, S. C., Novelli, P. C., Crotwell, M., Crotwell, A. M., Thoning, K. and Tans, P. P.: Seasonal climatology of CO2 across North America from aircraft measurements in the NOAA/ESRL Global Greenhouse Gas Reference Network, J. Geophys. Res. Atmos., 120(10), 5155-5190, 2015.

Tanaka, M., Nakazawa, T. and Aoki, S.: Concentration of atmospheric carbon-dioxide over japan, J. Geophys. Res. Ocean., 88(C2), 1339-1344, DOI: 10.1029/JC088iC02p01339, 1983.

Tanaka, T., Miyamoto, Y., Morino, I., Machida, T., Nagahama, T., Sawa, Y., Matsueda, H., Wunch, D., Kawakami, S. and Uchino, O.: Aircraft measurements of carbon dioxide and methane for the calibration of ground-based high-resolution Fourier Transform Spectrometers and a comparison to GOSAT data measured over Tsukuba and Moshiri, Atmos. Meas. Tech., 5(8), 2003-2012, 2012.

Tans, P. P., Conway, T. J. and Nakazawa, T.: Latitudinal distribution of the sources and sinks of atmospheric carbon-dioxide derived from surface observations and an atmospheric transport model, J. Geophys. Res. Atmos., 94(D4), 5151-5172, 1989.

Tans, P. P., Fung, I. Y. and Takahashi, T.: Observational constraints on the global atmospheric co2 budget, Science, 247(4949), 1431-1438, 1990.

Thoning, K. W., Tans, P. P. and Komhyr, W. D.: Atmospheric carbon-dioxide at Mauna Loa observatory. 2. Analysis of the NOAA GMCC data, 1974-1985, J. Geophys. Res. Atmos., 94(D6), 8549-8565, 1989.

Washenfelder, R. A., Toon, G. C., Blavier, J. F., Yang, Z., Allen, N. T., Wennberg, P. O., Vay, S. A., Matross, D. M. and Daube, B. C.: Carbon dioxide column abundances at the Wisconsin Tall Tower site, J. Geophys. Res. Atmos., 111, D22305, doi:10.1029/2006JD00715,4 2006.

Wofsy, S. C.: HIAPER Pole-to-Pole Observations (HIPPO): finegrained, global-scale measurements of climatically important atmospheric gases and aerosols, Philos. T. R. Soc. A, 369, 2073–2086, doi:10.1098/rsta.2010.0313, 2011.

Wunch, D., Wennberg, P. O., Toon, G. C., Keppel-Aleks, G., and Yavin Y. G.: Emissions of greenhouse gases from a North American megacity, Geophys. Res. Lett., 36, L15810, doi:10.1029/2009GL039825, 2009.

Wunch, D., Toon, G. C., Wennberg, P. O., Wofsy, S. C., Stephens, B. B., Fischer, M. L., Uchino, O., Abshire, J. B., Bernath, P., Biraud, S. C., Blavier, J. F. L., Boone, C., Bowman, K. P., Browell, E. V., Campos, T., Connor, B. J., Daube, B. C., Deutscher, N. M., Diao, M., Elkins, J. W., Gerbig, C., Gottlieb, E., Griffith, D. W. T., Hurst, D. F., Jimenez, R., Keppel-Aleks, G., Kort, E. A., Macatangay, R., Machida, T., Matsueda, H., Moore, F., Morino, I., Park, S., Robinson, J., Roehl, C. M., Sawa, Y., Sherlock, V., Sweeney, C., Tanaka, T. and Zondlo,

M. A.: Calibration of the Total Carbon Column Observing Network using aircraft profile data', Atmos. Meas. Tech., 3(5), 1351-1362, 2010.

Wunch, D., Toon, G. C., Blavier, J.-F. L., Washenfelder, R. A., Notholt, J., Connor, B. J., Griffith, D. W. T., Sherlock, V., and Wennberg, P. O.: The total carbon column observing network, Philosophical Transactions of the Royal Society - Series A: Mathematical, Physical and Engineering Sciences, 369(1943), 2087-2112, doi:10.1098/rsta.2010.0240, 2011.

Wunch, D., Wennberg, P. O., Messerschmidt, J., Parazoo, N. C., Toon, G. C., Deutscher, N. M., Keppel-Aleks, G., Roehl, C. M., Randerson, J. T., Warneke, T., and Notholt, J.: The covariation of Northern Hemisphere summertime CO2 with surface temperature in boreal regions, Atmos. Chem. Phys., 13, 9447–9459, doi:10.5194/acp-13-9447-2013,2013.